MRS Advances (2021) 6:54–60
https://doi.org/10.1557/s43580-021-00012-5

ORIGINAL PAPER

Evaluating magnesium alloy WE43 for bioresorbable coronary stent applications

Toh Yen Pang[1] · Jun Sheng Kwok[1] · Canh Toan Nguyen[1] · Kate Fox[1]

Received: 16 December 2020 / Accepted: 16 January 2021 / Published online: 8 February 2021

Abstract

Biodegradable stents, especially those composed of magnesium alloy-based materials, can provide a temporary scaffold that support vessels while naturally resorbing in the body after the targeted vessel heals, thereby preventing the restenosis and late thrombosis issues caused by their metallic predecessors. However, due to limitations in the intrinsic mechanical properties of magnesium, further investigation is required to optimize its degradation property, as well as the design, geometry and strut thickness to improve conformability in stent applications. This study aimed to investigate experimentally the degradation property of magnesium alloy WE43 and to optimize the stent geometry through parametric studies using the finite element method. Results of the degradation testing showed that the WE43 with a secondary polycaprolactone dip-coating offered a greater resistance to biodegradation and increased the lifespan of the stent. On average, the resistance to biodegradation increased by 5% in the WE43 magnesium alloy compared with its counterpart lacking any surface coating. The parametric studies have indicated that the stent with honeycomb geometry and a radial thickness of 0.15 mm had demonstrated promising mechanical performance with minimal dog-boning, foreshortening and recoil.

Keywords Magnesium alloy · Bioresorbable · Medical stents · Design optimization · Finite element analysis

Introduction

Recently, bioresorbable stent scaffolds have emerged as an ideal solution for restenosis and late thrombosis issues found in bare metallic stents. Magnesium (Mg) and magnesium alloys with controlled biosafety and good degradation behaviours have shown great promise in bioresorbable stent applications. Accordingly, Mg implants support tissue/artery healing, regeneration through their degrading process and, to their advantage, they constitute a biosafe process considering that Mg is an essential mineral in human metabolism [1, 2].

Commercial Mg alloys, including WE (Mg–RE–Zr) series (WE43, WE54), AZ (Mg–Al–Zn) series (AZ31, AZ91) and gravity-cast LAE442, were considered along with pure Mg as the suitable materials that not only have a significantly lower density, but also have mechanical strength ensuring sufficient radial resistance compared with other metallic stenting materials such as 316L stainless steel. More importantly, Mg alloys possess good biocompatibility and an adequate degradation property for stent applications [3–7].

Clinical studies have reported different stent design, geometry and strut thickness that can greatly affect mechanical integrity, biocompatibility and degradation that lead to reduced conformability [2, 8]. Efficiency of conformability depends on stent structures, including resistance to vessel pressures (radial strength), limited variation in length during expansion (foreshortening and recoil), a reduced "dog-boning" effect (i.e. non-uniform expansion of the stent) during expansion and the possibility of restenosis risk around the angioplasty site [2, 9, 10].

Previous studies have reported that while the LAE442 alloy possesses the greatest degradation resistance of all magnesium alloys, its strength is too low, even lower than pure magnesium, and necessitates a thicker strut design that leads to a larger crossing profile and prevents recoil. These thicker struts hinder the deliverability of the stent and disrupt the laminar blood flow, which increases the risk of restenosis and the platelet activation process leading to stent failure [9, 11]. The AZ series magnesium alloys, especially

✉ Kate Fox
kate.fox@rmit.edu.au

[1] School of Engineering, RMIT University, Melbourne, VIC 3000, Australia

Table 1 Comparison of ultimate tensile strength and biodegradability of magnesium alloys

Magnesium alloys	Ultimate tensile strength (MPa)	Resistance to biodegradation
Pure magnesium	199	Poor
Mg WE43	300	Average
Mg WE54	280	Fair
Mg AZ31	260	Very good
Mg AZ91	230	Good
Mg LAE442	154	Excellent

AZ91 and AZ31, have been reported to have good degradation resistance both in vitro and in vivo. However, they tend to release hydrogen upon degradation in physiological environments, leading to a significant increase in both pH and Mg^{2+} ion concentration, which will be harmful to living organisms [6, 12]. The WE series magnesium alloys, for example WE43 and WE54, were found to be stronger in terms of their mechanical strength, but they only performed slightly better in degradation resistance than the pure magnesium (Table 1). While WE43 and WE54 alloys possess marginally better biodegradation resistance, this resistance could be further enhanced with a corrosion-protective surface coating that lasts for six to twelve months in the body. This surface coating can act as a barrier to protect the magnesium underneath without sacrificing mechanical strength [7, 12].

Although some studies have investigated the mechanical and biodegradation behaviour of Mg WE43 alloy specimens [5, 13], there remain limitations in the understanding of Mg WE43 for the optimal design and development of metallic biodegradable stents. Therefore, it is necessary to investigate the Mg WE43 alloy degradation rate and optimize a stent geometry that can provide a temporary scaffold that resorbs once the artery heals. In this study, the degradation properties and mechanical performance of Mg WE43 were evaluated using finite element analysis (FEA) for stress distribution, dog-boning and recoil effects.

Materials and methods

Degradation test

Mg WE43 specimens were cut into cubes $10 \times 10 \times 10\ mm^3$ in volume and cleaned using a metal file to remove any pre-existing surface treatment and ensure homogeneous surface properties. In order to determine the degradation rate of the Mg WE43 alloy, specimens were immersed in 500 mL Hank's balanced salt solution in sterilized petri dishes according to the ASTM NACE/ASTM G31-12a standard [14]. Polycaprolactone (PCL) powders were dissolved in 100 mL of dichloromethane. The Mg WE43 alloy was then dip-coated in the fully dissolved PCL solution. The dipping process was repeated 3 times for each sample. The degradation analysis was performed on both coated samples and uncoated samples, the latter serving as a control. The weight of each sample was measured to calculate the percentage mass loss (Δm) in intervals of one week to four weeks according to Eq. (1):

$$\Delta m = \left(m_0 - m_{(t)}\right) \tag{1}$$

where m_o is the initial weight and $m_{(t)}$ is the weight of the specimen after every time internal.

Design analysis and material properties

FEA was adopted to perform the numerical investigation into the mechanical performance of the stent design by evaluating expansion recoil, foreshortening and dog-boning. Accordingly, the calculations of parameters are presented as the following equations [15]:

$$\text{Recoil}(\%) = \frac{D_{\text{expanded}} - D_{\text{recoil}}}{D_{\text{expanded}}} \times 100 \tag{2}$$

$$\text{Foreshortening}(\%) = \frac{L_{\text{crimped}} - L_{\text{expanded}}}{L_{\text{crimped}}} \times 100 \tag{3}$$

$$\text{Dogboning ratio} = \frac{D_{\text{distal}} + D_{\text{central}}}{D_{\text{distal}}} \tag{4}$$

The entire simulation model comprised a balloon, a hollow cylinder resembling the vessel wall and the stent, in which all three components were coaxially aligned as illustrated in Fig. 1. The balloon, which was used to inflate the

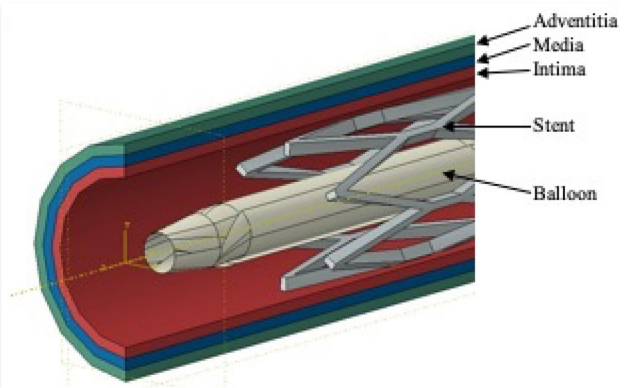

Fig. 1 Assembly of finite element model for stent deployment

stents, had a fully folded diameter of 0.98 mm with a total length of 23 mm. The balloon was modelled as a linear elastic material with a Young's Modulus of 1 GPa, a Poisson's ratio of 0.33 and a density of 1×10^{-9} kg/m^3 [16]. The vessels were modelled with three distinctive layers: 1. intima, 2. media and 3. adventitia, which were represented by three hyper-elastic strain functions in Abaqus software [16].

The stent was designed to have a honeycomb shape. The geometry of the stent was created using CATIA software and was chosen to undergo a parametric study (Fig. 2). The total unexpanded length of the stent was 17.64 mm with a central diameter of 2 mm. For the parametric study, the width of the struts and connectors was kept at 0.125 mm and 0.115 mm, respectively, and the crown angle was 22.056° throughout the entire stent, whereas the radial thickness was being manipulated between a range from 0.3 to 0.0125 mm while maintaining a constant central diameter. The stent was modelled with the Mg WE43 alloy material, which was adopted from [17] with a Young's Modulus of 16.162 GPa and a Poisson's ratio of 0.33. Its stress–strain curve is illustrated in Fig. 3.

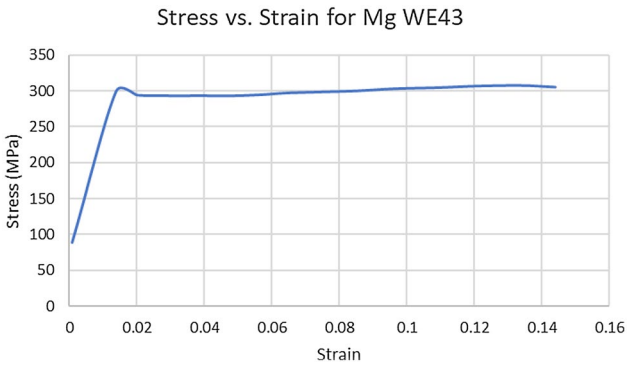

Fig. 3 The stress–strain curve of Mg WE43 alloy [17]

Crimping and expanding modelling

The stent and vessel were meshed using linear eight-node brick elements (C3D8I) with full integration. Hexahedral elements were chosen to mesh the stent and vessel as these provide better computational efficiency. Among the options for the hexahedral elements, C3D8 is prone to shear locking and C3D8R (reduced integration) is inferior compared with C3D8I (incompatible mode) in simulating bending behaviours. Therefore, C3D8I was selected to model the accurate crimping and expansion behaviour that involved large bending deformations [18]. The balloon was meshed with a combination of a four-node linear quadrilateral membrane (M3D4R) and three-node linear triangular membrane elements (M3D3) with a reduced integration scheme. Triangular elements were chosen to mesh the two ends of the tri-folded balloon as it was deemed more suitable for the geometry of the ends compared to quadrilateral elements.

Crimping simulation

To simulate the crimping process in which the stent was compressed to be placed on a catheter, the stent started at its original central radius (1 mm) and was then radially contracted until its inner radius reached the same value as the outer radius of the deflated balloon at 0.98 mm. This was carried out by applying uniform radial displacements across the external surface of the stent, which was oriented inward towards the axis of rotation (see Fig. 4).

Expansion simulation

The expansion simulation occurred after crimping, when the stent was expanded by inflating the balloon aligned inside the stent with a pneumatic fluid cavity pressure of 0.5 MPa applied on the interior wall of the balloon. The process of expansion was separated into four steps (see Fig. 5): 1. the balloon started at its originally deflated state (0.0 s); 2. inflation was then initiated linearly until it reached the specified magnitude for 0.006 s; 3. a constant pressure was maintained for a further 0.003 s to ensure the balloon reached a fully inflated diameter of 3 mm; and 4. finally, the balloon began to deflate for the next 0.005 s. These steps were done to study recoil and dog-boning.

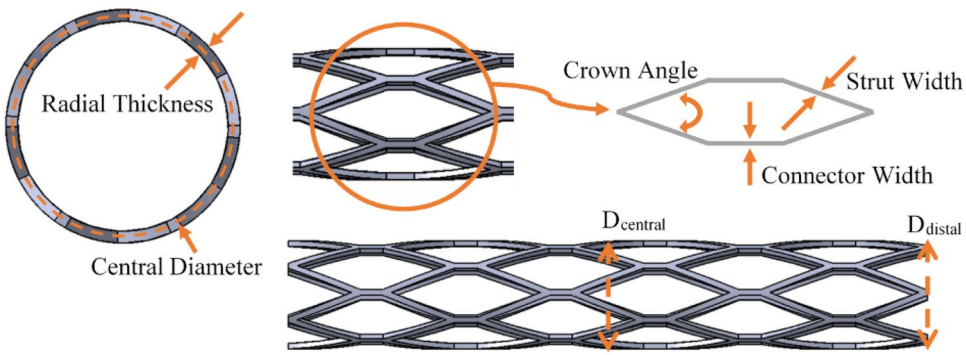

Fig. 2 Geometry and nomenclature of the honeycomb stent design

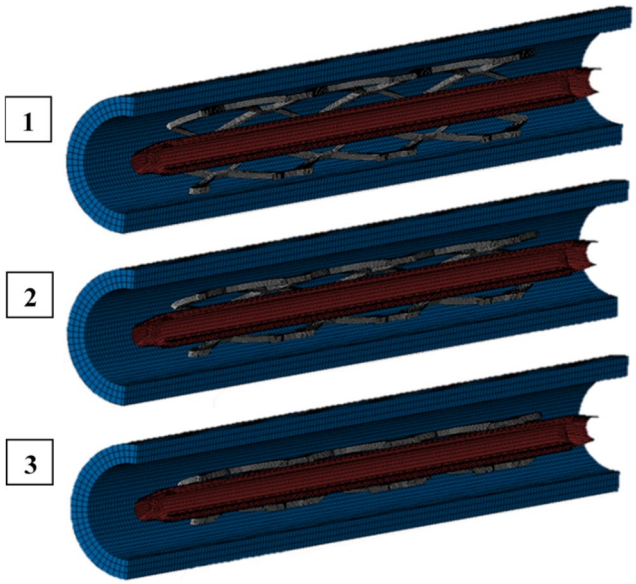

Fig. 4 The crimping process of the stent: (1) Stent at default diameter; (2) Stent began to crimp and (3) Stent inner diameter reached the outer diameter of balloon

Results and discussion

Figure 6 shows the percentage of weight loss of the coated and uncoated specimens over 4 weeks in the salt solutions. During the first week, the PCL coating provided a significant corrosion resistance to Mg WE43, whereas the uncoated specimens suffered a mean loss across the six samples of 15.9%, and the coated samples lost only 8.3% over the same period. The rate of the weight loss for the coated specimens with PCL was lower than uncoated specimen. The rate of the weight loss began to decline after 14 and 18 days for the uncoated and coated specimens, respectively.

The study found that after 25 days a PCL-coated WE43 implant would lose just under 37% of its weight and, given the trend of the degradation rate, it was predicted to last

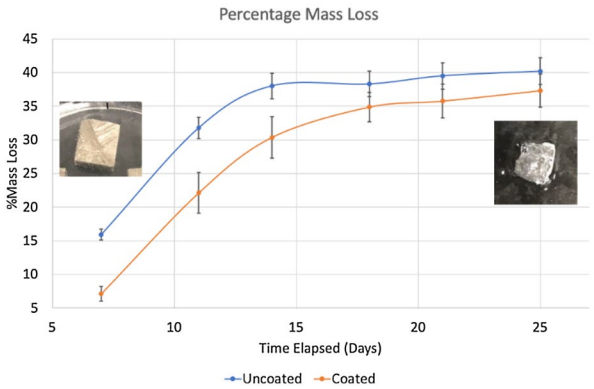

Fig. 6 The average percentage of mass loss for coated and uncoated Magnesium WE34 alloy specimens

at least 67 days/~2 months (assuming the trend is linear, i.e. the same amount of degradation occurs each day from day one). It is important to point out that the degradation rate is faster in vivo. The reaction between Mg and water molecules resulted in degradation of Mg^{2+} ions and blood flow constantly moving degradation products away from the surface of the stent [19]. Consequently, further in vivo testing is needed to understand the required lifespan of a stent in maintaining radial strength and vessel support for the critical three- to four-month period needed for vessel healing and, subsequently, for bioresorbing in about 12 months to avoid late stent thrombosis [8, 20, 21].

The ability to maintain radial strength and radial stiffness after being deployed inside vessels is one of the important factors to support the effectiveness of intravascular stents and their associated delivery systems. In this study, we explored the mechanical behaviour of Mg WE43 alloy during the crimping and expanding process. In the parametric study, a total of seven results were obtained from different radial thicknesses ranging between 0.025 mm up to 0.3 mm. It was clear that severe buckling began to occur when the radial thickness of the struts and connectors was reduced to

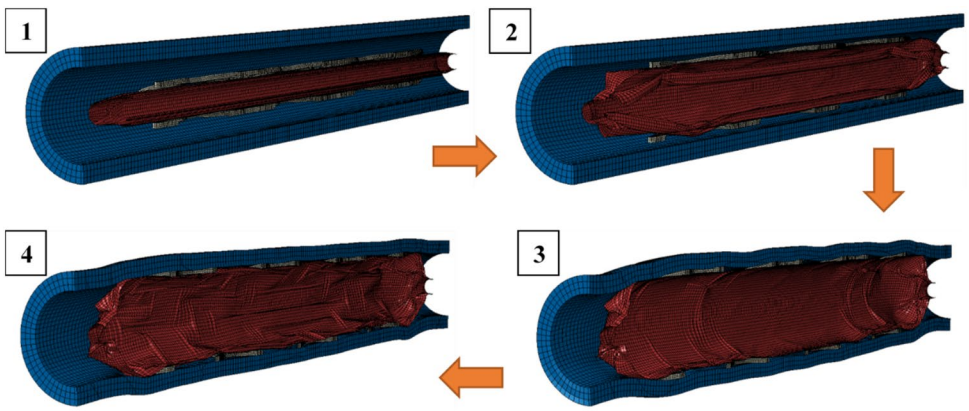

Fig. 5 Sectioned view of the expansion and deflation steps of the stent

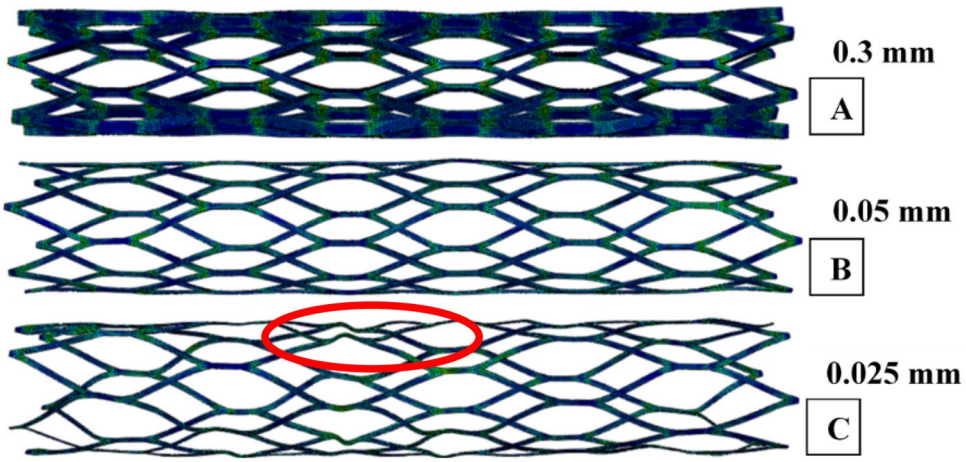

Fig. 7 Geometry of post-recoil stents for radial thickness of 0.3 mm (**a**), 0.05 mm (**b**) and 0.025 mm (**c**)

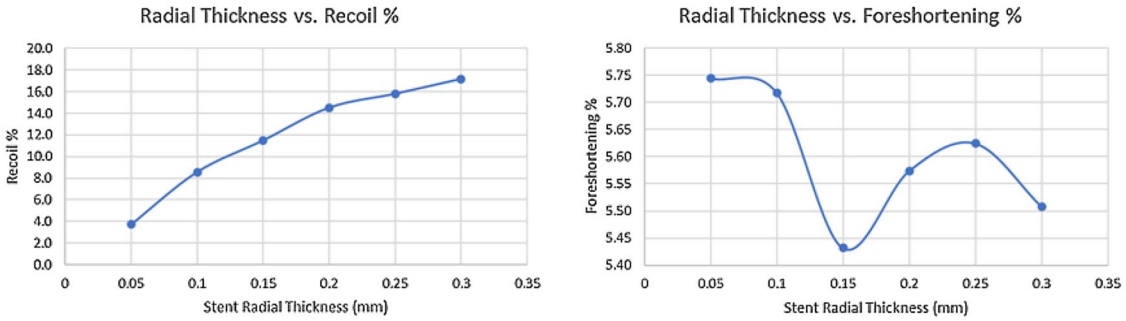

Fig. 8 Variation of radial thickness with the percentage of recoil and foreshortening

0.025 mm (see Fig. 7). Therefore, a thickness of 0.05 mm is the lowest possible radial thickness that can be used in further parametric studies.

Figure 8 shows that a further increase in radial thickness led to greater recoil from 0.025 to 0.3 mm and recoil increased substantially by 15.3%. However, for the foreshortening analyses, there was a drastic reduce in foreshortening between 0.05 and 0.3 mm and with an average of 5.6%. The FEA models showed that dog-boning effects are more significant during the initial expansion of the stent when the balloon begins inflating. The distal and central diameter during initial expansion were recorded, and consequently Eq. (4) was used to determine the dog-boning ratio for each radial thickness.

In Figs. 8 and 9, we noted the parameters to minimize foreshortening and dog-boning, which subsequently may reduce the associated risk of restenosis. The results indicate that the dog-boning effect was less prominent at a radial thickness between 0.15 and 0.2 mm with an average ratio of approximately 0.0122, although recoil increased with radial thickness. A lower recoil is preferable wherever possible. However, a 0.15 mm thickness has an exceptionally low foreshortening percentage at 5.43%, compared with the rest of the thicknesses, equivalent to a change of 0.974 mm

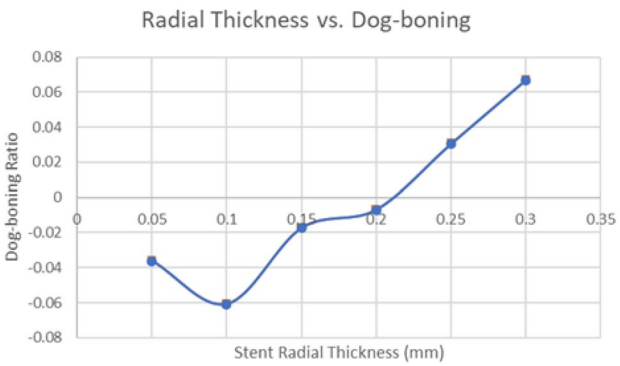

Fig. 9 Variation of dog-boning ratio with radial thickness

between the fully crimped length and fully expanded length. Hence, with both the dog-boning ratio and foreshortening falling under the desirable range, 0.15 mm was the most optimized radial thickness of the various thicknesses studied. Subsequently, the stress distributions and magnitudes were investigated on the 0.15 mm model. As shown in Fig. 10, the stresses were evenly distributed across the span of the stent, with peak stress appearing near the regions of the crowns reaching a maximum of 197.5 MPa. According

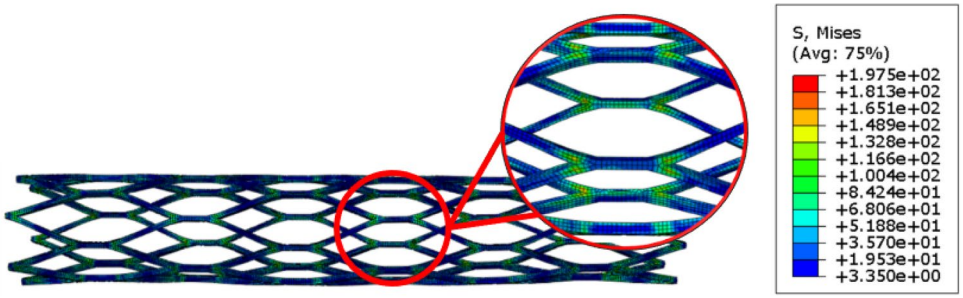

Fig. 10 Stress distribution and magnitude of honeycomb stent with thickness of 0.15 mm

to [17], well below the ultimate tensile strength of 308 MPa is deemed to have sufficient mechanical properties for this stent application.

These findings, while preliminary, suggest that there is room for innovation in the field of stent design. Future parametric design optimization can offer potential in improving the mechanical properties of stents in the body, which can lengthen the biocorrosion period of Mg WE43 in the blood vessel. The honeycomb "V"-shaped connector, while still exploratory, was able to redistribute the stress on the area usually most affected by cracking and the failures seen in previous bow-shaped designs [9]. The FEA provided the parametric investigation of optimizing the geometry and determining parameters for the stent design, whereas the crimping and expansion of the balloon was modelled with a constant pressure but, in reality, the balloon pressure was not uniform. Also, the time-dependent material behaviours, for example viscoelasticity and creep, were not considered in the study. These issues need to be considered in the future studies. However, they did not affect our general conclusions on the geometrical design of the stent.

Conclusions

The aim of this study was to find the optimum design for a stent made of Mg WE43 material using a honeycomb geometry. The degradation behaviour of Mg WE43 was experimentally investigated. The design parameters that affected foreshortening or dog-boning during the stent deployment were investigated using finite element analysis. It was found that adding a secondary polycaprolactone dip-coating was a viable method in increasing the in vivo life span of the degradation process and improving the mechanical behaviour and performance of Mg WE43 in stent applications. The parametric analysis concluded that a radial thickness of 0.15 mm for the honeycomb geometry demonstrated promising results in mechanical performance, with minimal dog-boning, recoil and foreshortening. While other studies have reported on the use of Mg WE43 for mechanical and corrosion testing, none has considered bioresorbable capabilities with polycaprolactone dip-coating method, which alters the resistance to degradation. There have been some studies that investigated the design optimization of bioresorbable stents with Mg WE43 materials to improve their effectiveness, but few studies have considered its mechanical properties fabricated via the additive manufacturing method, particularly the 3D printing process. The results of this study indicate that the combination of materials and the design to improve the performance of stent will assist in the future development of magnesium alloy-based bioresorbable stent applications.

Acknowledgements The authors thank the students who participated in this research. We also acknowledge the contributions of Prof. Cuie Wen for her generosity in providing Mg WE43 materials for testing.

Data availability The datasets generated during and/or analysed during the current study are available from the corresponding author on reasonable request.

Compliance with ethical standards

Conflict of interest On behalf of all authors, the corresponding author states that there is no conflict of interest.

References

1. W. Ding, Opportunities and challenges for the biodegradable magnesium alloys as next-generation biomaterials. Regen. Biomater. **3**, 79–86 (2016). https://doi.org/10.1093/rb/rbw003
2. R.W. Blair, N.J. Dunne, A.B. Lennon, G.H. Menary, Multi-objective optimisation of material properties and strut geometry for poly(L-lactic acid) coronary stents using response surface methodology. PLoS ONE (2019). https://doi.org/10.1371/journal.pone.0218768
3. R. Chalisgaonkar, Insight in applications, manufacturing and corrosion behaviour of magnesium and its alloys: a review. Mater. Today **26**, 1060–1071 (2020). https://doi.org/10.1016/j.matpr.2020.02.211
4. Z. Panahi, E. Tamjid, M. Rezaei, Surface modification of biodegradable AZ91 magnesium alloy by electrospun polymer nanocomposite: evaluation of in vitro degradation and cytocompatibility. Surf. Coat. Technol. **386**, 125461 (2020). https://doi.org/10.1016/j.surfcoat.2020.125461
5. E.L. Boland, R.N. Shirazi, J.A. Grogan, P.E. McHugh, Mechanical and corrosion testing of magnesium WE43 specimens for pitting corrosion model calibration. Adv. Eng. Mater. **20**, 1800656 (2018). https://doi.org/10.1002/adem.201800656

6. C. Liu, Z. Ren, Y. Xu, S. Pang, X. Zhao, Y. Zhao, Biodegradable magnesium alloys developed as bone repair materials: a review. Scanning **2018**, 9216314 (2018). https://doi.org/10.1155/2018/9216314
7. F. Witte, J. Fischer, J. Nellesen, C. Vogt, J. Vogt, T. Donath, F. Beckmann, In vivo corrosion and corrosion protection of magnesium alloy LAE442. Acta Biomater. **6**, 1792–1799 (2010). https://doi.org/10.1016/j.actbio.2009.10.012
8. J. Iqbal, J. Gunn, P.W. Serruys, Coronary stents: historical development, current status and future directions. Br. Med. Bull. **106**, 193–211 (2013). https://doi.org/10.1093/bmb/ldt009
9. M.M. Torki, S. Hassanajili, M.M. Jalisi, Design optimizations of PLA stent structure by FEM and investigating its function in a simulated plaque artery. Math. Comput. Simul. **169**, 103–116 (2020). https://doi.org/10.1016/j.matcom.2019.09.011
10. A. Khosravi, A. Akbari, H. Bahreinizad, M. Salimi Bani, A. Karimi, Optimizing through computational modeling to reduce dogboning of functionally graded coronary stent material. J. Mater. Sci. Mater. Med. **28**, 1–7 (2017). https://doi.org/10.1007/s10856-017-5959-7
11. D. Lim, S.-K. Cho, W.-P. Park, A. Kristensson, J.-Y. Ko, S.T.S. Al-Hassani, H.-S. Kim, Suggestion of potential stent design parameters to reduce restenosis risk driven by foreshortening or dogboning due to non-uniform balloon-stent expansion. Ann. Biomed. Eng. **36**, 1118–1129 (2008). https://doi.org/10.1007/s10439-008-9504-1
12. Z.-Z. Yin, W.-C. Qi, R.-C. Zeng, X.-B. Chen, C.-D. Gu, S.-K. Guan, Y.-F. Zheng, Advances in coatings on biodegradable magnesium alloys. J. Magn. Alloys (2020). https://doi.org/10.1016/j.jma.2019.09.008
13. W. Wu, L. Petrini, D. Gastaldi, T. Villa, M. Vedani, E. Lesma, B. Previtali, F. Migliavacca, Finite element shape optimization for biodegradable magnesium alloy stents. J. Biomed. Eng. Soc. **38**, 2829–2840 (2010). https://doi.org/10.1007/s10439-010-0057-8
14. ASTM Nace/ASTMG31-12a, *Standard Guide for Laboratory Immersion Corrosion Testing of Metals* (West Conshohocken, ASTM International, 2012).
15. C. Chen, J. Chen, W. Wu, Y. Shi, L. Jin, L. Petrini, L. Shen, G. Yuan, W. Ding, J. Ge et al., In vivo and in vitro evaluation of a biodegradable magnesium vascular stent designed by shape optimization strategy. Biomaterials **221**, 119414 (2019). https://doi.org/10.1016/j.biomaterials.2019.119414
16. A. Schiavone, T.-Y. Qiu, L.-G. Zhao, Crimping and deployment of metallic and polymeric stents—finite element modelling. Vessel Plus **1**, 12–21 (2017). https://doi.org/10.20517/2574-1209.2016.03
17. N.A. Zumdick, L. Jauer, L.C. Kersting, T.N. Kutz, J.H. Schleifenbaum, D. Zander, Additive manufactured WE43 magnesium: a comparative study of the microstructure and mechanical properties with those of powder extruded and as-cast WE43. Mater. Charact. **147**, 384–397 (2019). https://doi.org/10.1016/j.matchar.2018.11.011
18. D. Systèmes, *Getting Started with Abaqus*, Keywords. (Providence, Dassault Systèmes Simulia Corp, 2018).
19. S. Borhani, S. Hassanajili, S.H. Ahmadi Tafti, S. Rabbani, Cardiovascular stents: overview, evolution, and next generation. Progress Biomater. **7**, 175–205 (2018). https://doi.org/10.1007/s40204-018-0097-y
20. S. Verheye, J.A. Ormiston, J. Stewart, M. Webster, E. Sanidas, R. Costa, J.J.R. Costa, D. Chamie, A.S. Abizaid, I. Pinto et al., A next-generation bioresorbable coronary scaffold system: from bench to first clinical evaluation: 6- and 12-month clinical and multimodality imaging results. JACC Cardiovasc. Interv. **7**, 89–99 (2014). https://doi.org/10.1016/j.jcin.2013.07.007
21. S.-H. Kang, I.-H. Chae, J.-J. Park, H.S. Lee, D.-Y. Kang, S.-S. Hwang, T.-J. Youn, H.-S. Stent. Kim, Thrombosis with drug-eluting stents and bioresorbable scaffolds: evidence from a network meta-analysis of 147 trials. JACC Cardiovasc. Interv. **9**, 1203–1212 (2016). https://doi.org/10.1016/j.jcin.2016.03.038